Journal of Ginseng Research 46 (2022) 572–584

Contents lists available at ScienceDirect

Journal of Ginseng Research

journal homepage: https://www.sciencedirect.com/journal/journal-of-ginseng-research

Research Article

Ginsenoside compound K reduces the progression of Huntington's disease via the inhibition of oxidative stress and overactivation of the ATM/AMPK pathway

Kuo-Feng Hua [a, b, c, 1], A-Ching Chao [d, e, 1], Ting-Yu Lin [f], Wan-Tze Chen [g], Yu-Chieh Lee [h], Wan-Han Hsu [h], Sheau-Long Lee [h], Hsin-Min Wang [i], Ding-I. Yang [g], Tz-Chuen Ju [f, j, *]

[a] Department of Pathology, Tri-Service General Hospital, National Defense Medical Center, Taipei, Taiwan
[b] Department of Biotechnology and Animal Science, National Ilan University, Ilan, Taiwan
[c] Department of Medical Research, China Medical University Hospital, China Medical University, Taichung, Taiwan
[d] Department of Neurology, Kaohsiung Medical University Hospital, Kaohsiung, Taiwan
[e] Department of Neurology, College of Medicine, Kaohsiung Medical University, Kaohsiung, Taiwan
[f] Department of Animal Science and Biotechnology, Tunghai University, Taichung, Taiwan
[g] Institute of Brain Science and Brain Research Center, National Yang Ming Chiao Tung University, Taipei, Taiwan
[h] Wellhead Biological Technology Corp., Taoyuan, Taiwan
[i] 6-Shun Clinic, Tainan, Taiwan
[j] National Defense Medical Center, Taipei, Taiwan

ARTICLE INFO

Article history:
Received 11 July 2021
Received in revised form
16 October 2021
Accepted 4 November 2021
Available online 11 November 2021

Keywords:
AMP-Activated protein kinase
Ataxia-telangiectasia mutated
Panax ginseng, ginsenoside
Huntington's disease

ABSTRACT

Background: Huntington's disease (HD) is a neurodegenerative disorder caused by the expansion of trinucleotide CAG repeat in the Huntingtin (*Htt*) gene. The major pathogenic pathways underlying HD involve the impairment of cellular energy homeostasis and DNA damage in the brain. The protein kinase ataxia-telangiectasia mutated (ATM) is an important regulator of the DNA damage response. ATM is involved in the phosphorylation of AMP-activated protein kinase (AMPK), suggesting that AMPK plays a critical role in response to DNA damage. Herein, we demonstrated that expression of polyQ-expanded mutant Htt (mHtt) enhanced the phosphorylation of ATM. Ginsenoside is the main and most effective component of *Panax ginseng*. However, the protective effect of a ginsenoside (compound K, CK) in HD remains unclear and warrants further investigation.

Methods: This study used the R6/2 transgenic mouse model of HD and performed behavioral tests, survival rate, histological analyses, and immunoblot assays.

Results: The systematic administration of CK into R6/2 mice suppressed the activation of ATM/AMPK and reduced neuronal toxicity and mHTT aggregation. Most importantly, CK increased neuronal density and lifespan and improved motor dysfunction in R6/2 mice. Conversely, CK enhanced the expression of Bcl2 protected striatal cells from the toxicity induced by the overactivation of mHtt and AMPK.

Conclusions: Thus, the oral administration of CK reduced the disease progression and markedly enhanced lifespan in the transgenic mouse model (R6/2) of HD.

1. Introduction

Huntington's disease (HD) is a neurodegenerative disorder caused by the expansion of the trinucleotide CAG repeat in the Huntingtin (*Htt*) gene [1]. When the number of CAG repeats is > 36, the translated polyQ-expanded mutant HTT (mHTT) protein forms aggregates [2–4]. The abnormal accumulation of polyQ-expanded mHtt also leads to aggregate formation in the nuclei of microglia, neurons, and different types of peripheral cells [2,5–7]. Further,

* Corresponding author. Department of Animal Science and Biotechnology, Tunghai University, No. 1727, Sec. 4, Taiwan Blvd., Xitun Dist., Taichung City, 407224, Taiwan.
E-mail address: tzchuen@thu.edu.tw (T.-C. Ju).
[1] These authors contributed equally.

https://doi.org/10.1016/j.jgr.2021.11.003

mHtt promotes protein misfolding; thus, it inhibits the activity of the proteasome, dysregulates transcription, impairs synaptic functions, induces oxidative stress, and degenerates axons, eventually leading to neurodegeneration and neuronal loss [5,8–10]. However, no effective treatment for HD is currently available.

The AMP-activated protein kinase (AMPK) is an energy sensor that sustains cellular energy homeostasis by regulating the downstream target genes [11]. AMPK is a heterotrimeric complex composed of α, β, and γ subunits. AMPK can be activated by cAMP-dependent kinase, calmodulin-dependent protein kinase [12], liver kinase B1 (LKB1), and Ca^{2+}/calmodulin-dependent protein kinase II [13,14]. The substrates of AMPK are involved in energy metabolism and different cellular processes [15]. AMPK activation increases ROS formation, subsequently causing mitochondrial damage and apoptosis [16,17]. The roles and regulation of AMPK in HD pathogenesis, including oxidative stress and DNA damage, have been investigated. We previously reported that AMPK activation occurs in striatal neurons of R6/2 mice and patients with HD. In the past several years, the correlation between oxidative stress and DNA damage has been documented. ATM is involved in the phosphorylation of AMPK. Fu et al. reported that activation of ATM by etoposide induces ROS production and mitochondrial biogenesis through the phosphorylation/activation of AMPK. Overexpression of a 43Q-GFP fusion protein increases ROS production and ATM activity, and subsequently evokes ATM-dependent DNA damage in PC12 cells [18]. Suzuki et al. reported that IGF-1 induced AMPK activation in human and mouse fibroblast cells via LKB1-independent and ATM-dependent manner [19]. Thus, oxidative stress might promote mitochondrial biogenesis via the DNA damage, ATM and AMPK pathway [20]. We previously characterized the positive feedback loops between the activation of AMPK-α1 and increased oxidative stress that contributes to the disease progression in HD [17]. However, the role of the correlation between DNA damage and AMPK-α in HD has not been determined.

Panax ginseng has been used as a medicine in Asia for various diseases, including neurodegenerative and aging disorders (such as HD, Alzheimer's disease, amyotrophic lateral sclerosis, Parkinson's disease, and multiple sclerosis) [21]. Ginsenoside is the main and most effective component of *Panax ginseng*. Several ginsenoside compounds have been identified and used to prevent HD. Compound K (CK), an intestinal bacterial metabolite of *Panax ginseng* protopanaxadiol saponins, is one of the major deglycosylated metabolites of ginsenosides that can be absorbed in the systemic circulation. CK from *Panax ginseng* (20-O-β-D-glucopyranosyl-20(S)-protopanaxadiol) was prepared according to our US patent (US7932057B2). Recently, the potential protective effect of CK and the underlying mechanisms in R6/2 mice (transgenic mouse model of HD) remain unclear. In this study, we tested the protective action of CK in HD pathogenesis that involves ATM/AMPK dependent pathway.

2. Materials and methods

2.1. Cell culture and transfection

Striatal progenitor cell lines (ST*Hdh*^{Q7} and ST*Hdh*^{Q109}) were provided by Dr. Elena Cattaneo and Yijuang Chern. The conditionally immortalized striatal neuronal progenitor cells, derived from wild-type mice (ST*Hdh*^{Q7}) or knock-in mice (ST*Hdh*^{Q109}), express endogenous normal Htt harboring seven and 109 glutamines, respectively. These cells were kept in an incubation chamber at 33 °C and 5% CO_2 in Dulbecco's Modified Eagle's Medium (Thermo Fisher Scientific Inc. Waltham, MA, USA) supplemented with 10% fetal bovine serum (HyClone™ Fetal Bovine Serum, USA) [22]. Only the cells with passage number <20 were used. Small interfering RNA (siRNA) was obtained from RNAiCore in the Biomedical Translation Research Center (BioTReC), Sinica, Taiwan. Cells were transfected using lipofectamine 2000 according to the manufacturer's protocol (LF2000, Thermo Fisher Scientific Inc.) [22]. Mirin, Ku55933, camptothecin (CPT) was obtained from Sigma-Aldrich (St. Louis, MO, USA).

2.2. Cell death assays

Cell death was quantified using the MTT reduction assay 3-[4,5-dimethylthiazol-2-yl]-2,5-diphenyltetrazolium bromide (MTT; Sigma-Aldrich) and Alamar Blue assay (Thermo Fisher Scientific Inc). Fluorescence at excitation 570 nm/emission 600 nm was measured using a OPTImax tunable microplate reader (Molecular Devices) [23].

2.3. Measurement of ROS in vitro

Cellular ROS analysis was performed as previously described [17] by the oxidant-sensing probe 2′,7′-dichlorodihydrofluorescein diacetate (H_2DCFDA; Molecular Probes, Inc., Eugene, OR, USA). Briefly, cells were incubated in a culture medium containing H_2DCFDA (50 μM) for 30 min at 33 °C. Cells were washed thrice in Locke's buffer, lysed in Tris-ethylenediaminetetraacetic acid (EDTA) buffer containing 0.2% Triton X-100 for 10 min, and centrifuged at 15,000×*g* for 5 min at 4 °C. Fluorescence intensity (at excitation and emission wavelengths of 488 and 510 nm, respectively) was measured in the supernatant (cytoplasmic fraction) using a fluorescence plate reader (Thermo Fisher Scientific Inc.).

2.4. Immunoprecipitation

Immunoprecipitation was performed as previously described [24]. Briefly, cells were lysed with ice-cold Tris–NaCl–EDTA (TNE) buffer and incubated with an anti-AMPK-α1 antibody (Novus Biologicals, Littleton, CO, USA) for 1 h at 4 °C on a rolling wheel. The complexes were then mixed with protein A beads (Sigma-Aldrich) and incubated for 1 h at 4 °C. The immunocomplex was extensively washed with ice-cold TNE buffer and analyzed by SDS-PAGE and western blotting.

2.5. SDS-PAGE and western blotting

Western blot analysis was performed as previously defined [24]. The primary antibodies anti-phosphor-ATM, anti-Bcl2, and anti-phosphor-AMPK antibodies (Cell Signaling Technology, Danvers, MA, USA) were used; anti-γH2AX, anti-mHtt, anti-V5, and anti-actin antibodies (Millipore, Billerica, MA, USA) were used. Immunoreactive signals on the blots were identified using an enhanced chemiluminescence (ECL) detection system (PerkinElmer Life and Analytical Sciences, Boston, MA, USA). The protein band quantifications were analyzed using the ImageJ Gel Analysis program.

2.6. Animals and CK treatment

Male transgenic R6/2 mice (B6CBA-Tg(HDexon1)62Gpb/3J), which express exon 1 of the human huntingtin gene with 120 ± 5 CAG repeat expansions, were received from the Jackson Laboratory (Bar Harbor, ME, USA; stock number 006494) and mated with female control mice (B6CBAFI/J). Posterity were identified by the PCR genotyping and sequencing technique of genomic DNA using primers located in the transgene (5′-CCGCTCAGGTTCTGCTTTTA-3′ and 5′-GGCTGAGGAAGCTGAGGAG-3′). All experimental measures involving animals were accepted by the Ilan University Animal Ethics Committee (permit number 106-8). Mice arrived at the Ilan

University Animal Care Facility at 4 wks of age, were housed in groups of five animals, and were maintained under controlled conditions with a 12-h light/dark cycle and with food and water ad libitum. Experiments were planned and completed according to the 3Rs principles, which comprise the decrease of animal excruciation and number of mice used. For treatment with CK, transgenic R6/2 mice received daily CK dose (30 or 60 mg/kg of body weight, oral gavage administration) or vehicle for 5 wks, starting from 7 wks of age. Behavioral assays were performed between 5 and 12 wks of age.

2.7. Behavioral tests

2.7.1. Rotarod performance

The motor coordination was assessed using a Rotarod apparatus (UGO BASILE, Comerio, Italy) at a constant speed (12 rpm for 2 min). All mice were tested three times per week. Each test session comprised three trials for each mouse. The latency to fall from the rotating rod, up to a maximum of 2 min, was recorded for each trial. Weekly maximum performance for each mouse was used for statistical analysis.

2.7.2. Clasping

At 12 weeks of age, the position of the hind limbs upon tail suspension was observed for 10 s. A score of 0 was assigned if the hind limbs were consistently splayed outwards, away from the abdomen. A score of 1 was assigned if one hind limb was retracted toward the abdomen for more than 50% of the 10-s observation period. A score of 2 was assigned if both hind limbs were partially retracted toward the abdomen for more than 50% of the 10-s observation period. Finally, a score of 3 was assigned if the hind limbs were entirely retracted and touching the abdomen for more than 50% of the 10-s observation period.

2.8. Measurement of ROS in brain tissue

To analyze ROS production in in vivo tissues, coronal sections of 20 μm were cut (HM430, Microm, Walldorf, Germany). Brain sections were keep with CellROX™ Green Reagent (5 μM; Molecular Probes, Inc.) for 30 min. For the quantification of the images, the acquisition was performed using laser confocal microscopy (LSM810, Carl Zeiss MicroImaging) and analyzed using the MetaMorph imaging system (Universal Imaging).

2.9. Immunohistochemistry and quantitation

Brain sections were immunohistochemically stained as described before [25]. Briefly, brain sections were incubated overnight with the appropriate primary antibody in PBS containing 5% normal goat serum at 4 °C, then incubated with the corresponding secondary antibody for 2 h at room temperature. The following primary antibodies and concentrations were used: anti-phosphor-ATM (1:100), anti-phosphor-AMPK (1:200), anti-NeuN (1:500), and anti-mHtt (1:250) (Millipore). Secondary antibodies were conjugated to Alexa Fluor 488, Alexa Fluor 568, or Alexa Fluor 633. Nuclei were stained with 4',6-diamidino-2-phenylindole (DAPI). The slides were mounted using Vectashield (Vector Laboratories, Burlingame, CA, USA). To determine the number of neurons in the striatum, nine frames from three sections spaced evenly throughout the striatum (interaural 5.34 mm/bregma 1.54 mm to interaural 3.7 mm/bregma −0.1 mm) were analyzed for each animal by an investigator blinded to the experimental conditions; at least 500 cells from each animal were counted and measured. For the quantification of the images, the acquisition was performed using laser confocal microscopy (LSM810, Carl Zeiss MicroImaging) and analyzed using the MetaMorph imaging system (Universal Imaging).

2.10. Filter retardation assay

The mHtt aggregates were measured as described before [24]. The primary antibodies anti-Htt and anti-actin antibodies (Millipore).

2.11. Statistical analysis

Results are expressed as mean ± standard error of the mean (SEM). Each experiment was duplicate more than three times. Comparisons among several groups were evaluated by one-way analysis of variance followed by Dunnett's post-hoc test. Differences between treatment means were deliberate statistically significant at $P < 0.05$.

3. Results

3.1. Selective activation of ATM in striatal neurons in R6/2 mice

To evaluate the role of ATM in HD pathogenesis, we first assessed the activation of ATM in the brains of mice with HD. The phosphorylation (activation) level of ATM (ATM-p) significantly increased in the striatum of R6/2 mice, but not in that of WT mice (Fig. 1A and B). The activation of ATM was disease-stage-dependent in R6/2 mice; in the late stage, the phosphorylation (activation) level of ATM and mHtt aggregation significantly raised in the striatum of R6/2 mice (Fig. 1A and C), whereas the ATM inhibitor Ku55933 reduced the activation level of ATM (ATM-p) and mHtt aggregates in R6/2 mice (Fig. 1D–F).

3.2. AMPK-α is a downstream target of ATM in striatal cells

Numerous kinases are known to control the phosphorylation of AMPK, including ATM in PC12 and human embryonic kidney cells [18]. Here, we showed that AMPK-α was phosphorylated by ATM, which probable mediate the aberrant phosphorylation of AMPK in HD. We determined the phosphorylation of ATM in ST*Hdh*^{Q7} or ST*Hdh*^{Q109} cells. The phosphorylation of ATM was higher in ST*Hdh*^{Q109} cells more than that in ST*Hdh*^{Q7} cells (Fig. 2A). Two ATM inhibitors Ku55933 and Mirin (Fig. 2A) and an ATM-siRNA (Fig. 2B) significantly reduced the overactivation of ATM in ST*Hdh*^{Q109} cells. The knockdown efficacies of ATM-siRNA in ST*Hdh*^{Q109} cells are shown in Fig. S1. We next assessed the interplay between AMPK and ATM in striatal neurons in HD. ATM inhibitors blocked the activation of AMPK in ST*Hdh*^{Q109} cells (Fig. 2C). Consistent with the significance of ATM in the phosphorylation of AMPK, we discover that the phosphorylation level of AMPK at Thr^{172} was lower in the cells transfected with ATM-siRNA (Fig. 2D). Reportedly, sequence S/TQ is an essential amino acid for substrate recognition by ATM kinase [26]. We identified substrates for ATM and RAD3-related (ATR) by recognizing the phosphorylated serine or threonine in the S/TQ motif. Immunoprecipitation of AMPK-α1 and Western blot analysis using ATM-substrate phosphorylated antibody were performed. ATM-substrate phosphorylation in ST*Hdh* ^{Q7}cells was significantly lower than that in ST*Hdh* ^{Q109} cells (Fig. 2E). ATM-siRNA and ATM inhibitor (Ku55933) reduced the substrate phosphorylation in ST*Hdh*^{Q109} cells (Fig. 2F and G). We found a SQ motif in AMPK-α1 at Ser^{413} and hydrophobic amino acids at N-3 [Fig. S2, One ATM phosphorylation site (S413) is shown in black]. To assess whether ATM phosphorylates AMPK-α1 through SQ motif, we created AMPK-α1 variants, in which the Ser^{413} residue was mutated into alanine (AMPK-α1-S413A-V5; S413A). Cells were transfected with

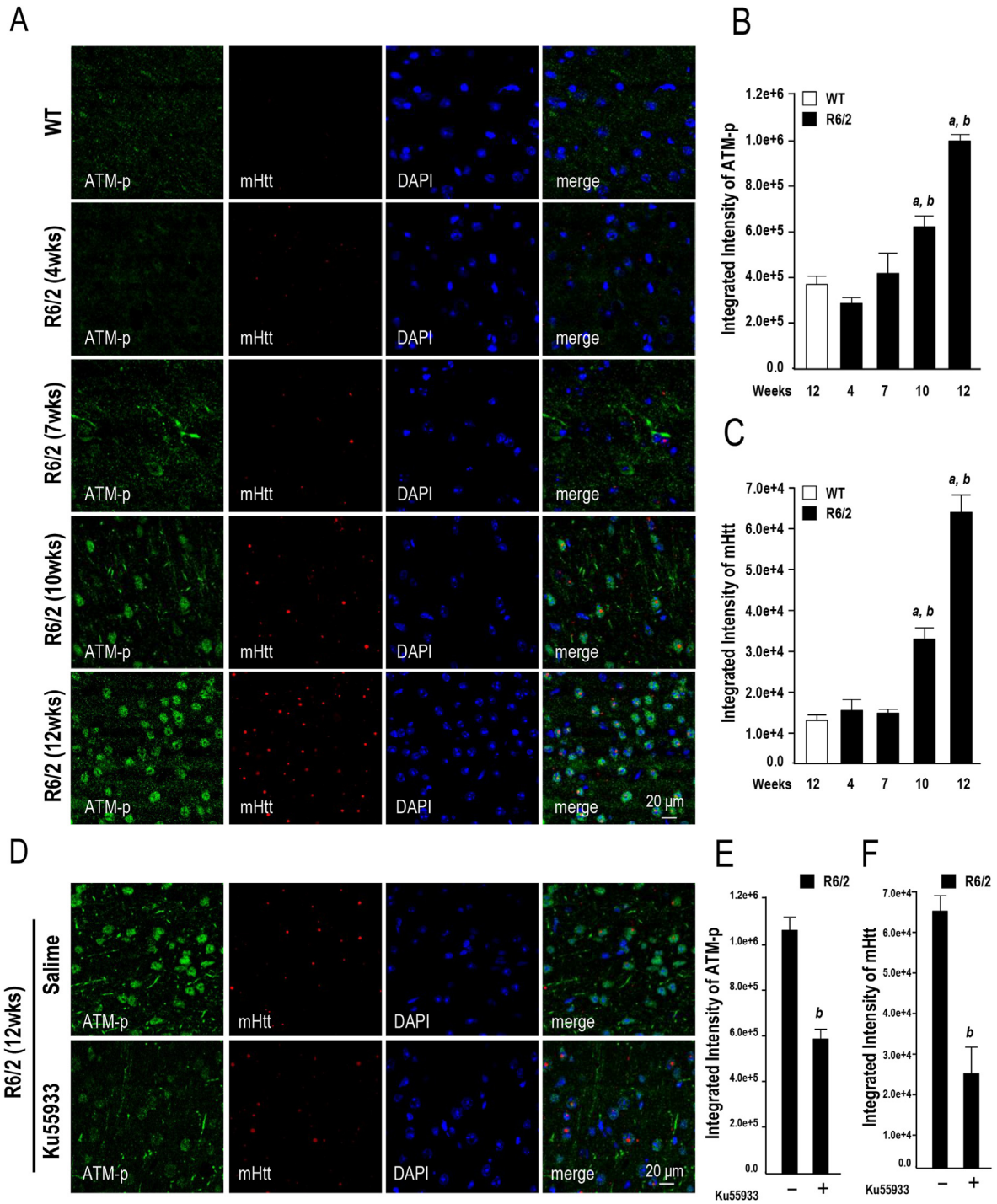

Fig. 1. Expression of polyQ-expanded mutant huntingtin enhances the phosphorylation of ATM.

the indicated construct [AMPK-α1-WT-V5 (WT) and AMPK-α1-S413A-V5 (S413A)] for 48 h. We subsequently immunoprecipitated AMPK-α1 using the V5 antibody. A dominant-negative mutant of AMPK-α1 at Ser^{413} (S413A/V5) significantly reduced the ATM-substrate phosphorylation level in STHdh^{Q109} cells (Fig. 2G). Thus, these results suggest that ATM phosphorylated AMPK-α1 through SQ motif at Ser^{413}. In addition, Ser^{413} is important in the activation of AMPK-α1 at Thr^{172}.

3.3. mHtt renders striatal neurons vulnerable to DNA damage induced by an ATM activator

We have demonstrated that the expression of mHtt enhances the phosphorylation levels of ATM and AMPK (Figs. 1 and 2). ATM regulates DNA repair through the phosphorylation of the Ser^{139} residue of H2AX [27,28]. Here we first showed that an ATM activator camptothecin (CPT) and doxorubicin (DOX) time-dependently activated ATM in the STHdh^{Q109} cells with concomitant phosphorylation of AMPK-α1 (Fig. 3A and Fig. S3).

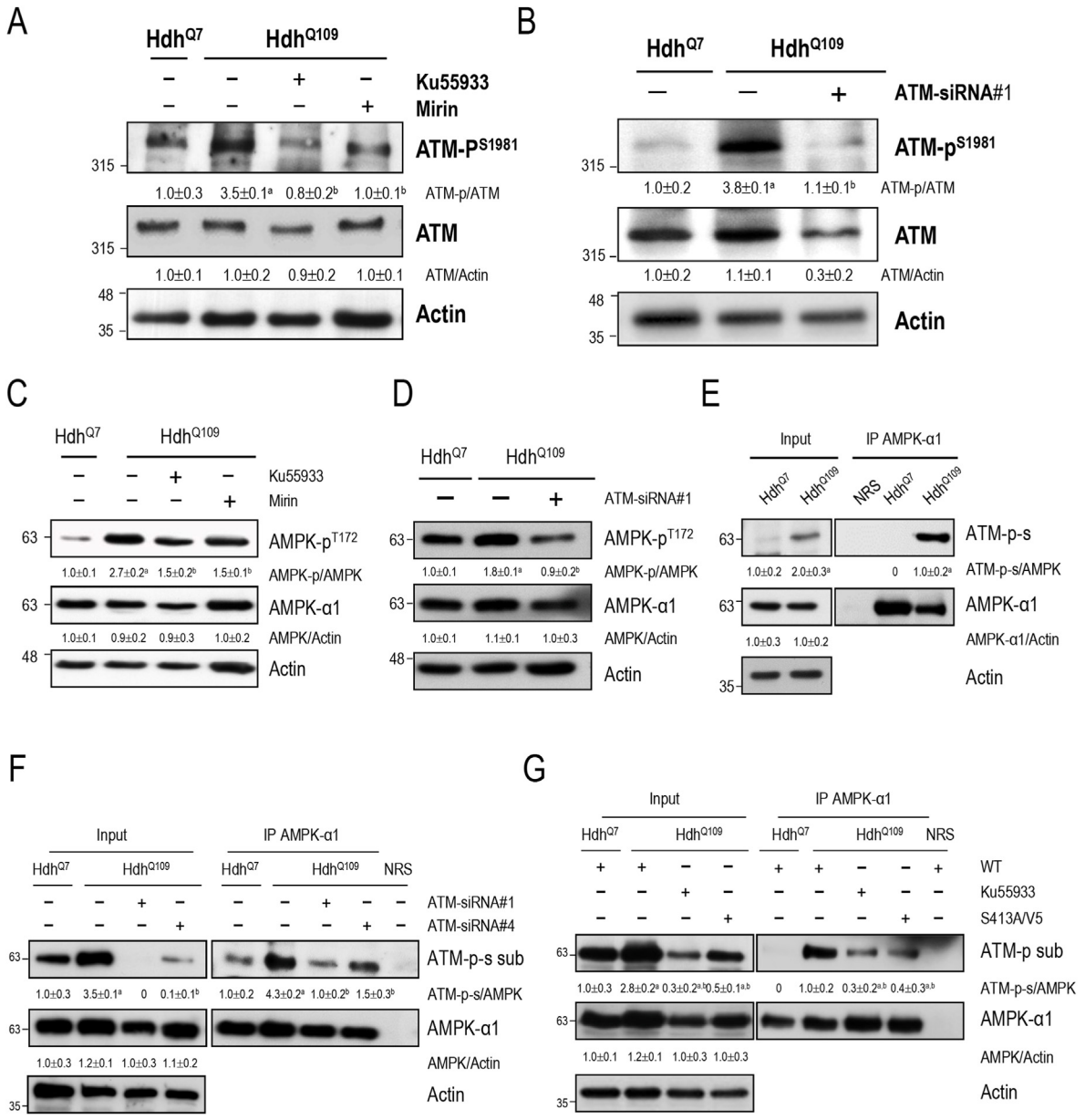

Fig. 2. AMPK-α1 is a downstream target of ATM in striatal cells.

Immunofluorescence confocal microscopy confirmed colocalization of CPT and DOX-induced ATM-p and AMPK-p (Fig. 3B and Fig. S3B). Furthermore, CPT and DOX time-dependently activated H2AX with an increased γH2AX level in the mHtt-expressing ST*Hdh*^{Q109} cells; CPT and DOX also increased γH2AX level in the control ST*Hdh*^{Q7} cells, albeit to a much lesser extent (Fig. 3C and Fig. S3A). Immunofluorescence microscopy confirmed the heightened expression of γH2AX upon exposure to CPT in the ST*Hdh*^{Q109} cells (Fig. 3D).

3.4. CK significantly reduces cytotoxicity and oxidative stress in mHtt-expressing cells

Next, we assessed the protective effect of CK in HD. The cytoprotection of CK in striatal cells was first assessed by MTT reduction assay (Fig. 4A) and Alamar Blue assay (Fig. 4B) in mHtt-expressing cells. Our results show that CK blocked the death of ST*Hdh*^{Q109} cells (Fig. 4A and B). Higher ROS levels were examined in the ST*Hdh*^{Q109} cells compared with ST*Hdh*^{Q7} cells, whereas CK markedly decreased mHtt induced ROS in ST*Hdh*^{Q109} cells (Fig. 4C).

3.5. Oral administration of CK halts disease progression in a transgenic mouse model (R6/2) of HD

To evaluate the actions of CK, we tested the effect of oral administration of CK in R6/2 mice for 5 wks from the age of 7 wks. Schematic representation of the experimental procedure and behavioral test (Fig. 5A). CK rescued weight decrease of the R6/2 mice (Fig. 5B). CK also reduced motor dysfunction as assessed by the rotarod test (Fig. 5C) and clasping scores (Fig. 5D). Most importantly, oral administration of CK extended the lifespan of mice with HD (Fig. 5F). In parallel with the improved motor dysfunction, CK markedly enhanced neuronal survival in the striatum of mice with HD. This was based on immunohistochemical

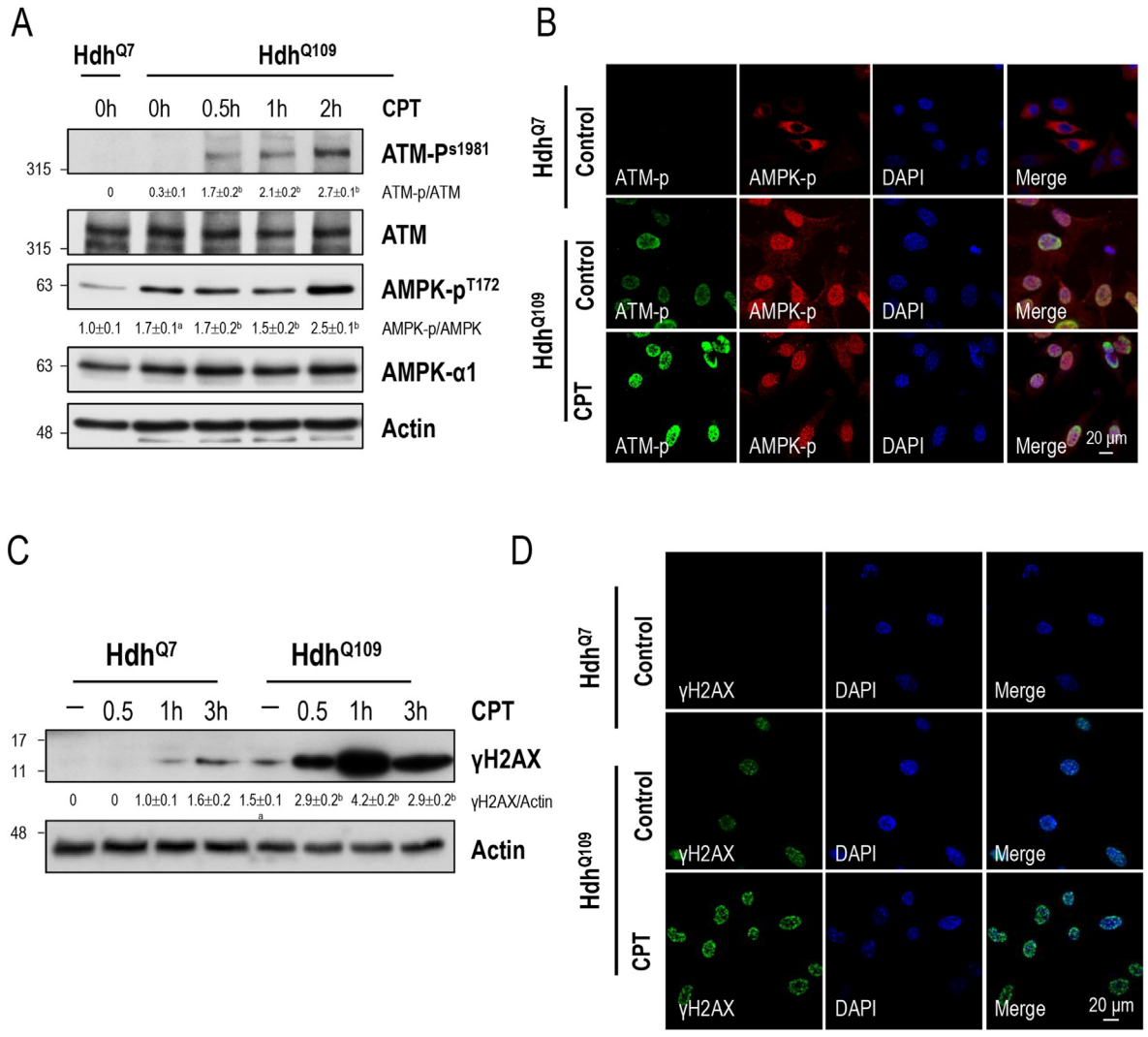

Fig. 3. An ATM activator (CPT) triggers ATM and AMPK activation in ST*Hdh*^{Q109} cells.

staining (Fig. 6A), quantitative analyses of striatal NeuN^{+} neuron density (Fig. 6B) shown in Fig. 6A (green), and western blotting to detect striatal NeuN expression (Fig. 6D). Consistent with an inverse relationship between neuronal survival and mHtt aggregation, quantitative analyses of signal intensities of mHtt (Fig. 6C) on the immunostaining micrographs [Fig. 6A (red)] and filter retardation assay (Fig. 6E) revealed that oral administration of CK significantly reduced the formation of mHtt aggregates in mice with HD.

3.6. CK protects striatal cells against mHtt-mediated neuronal cell death and interferes with the detrimental action of ROS, ATM, and AMPK

We previously established that, AMPK-α1 is abnormally activated by mHtt and exerts a harmful effect on neuronal survival through the inhibition of the pro-survival protein Bcl2 [24], and we also suggested that a positive feedback loops regulation between the formation of ROS and phosphorylation of AMPK-α1 in HD [17]. Here, we demonstrated that treatment with CK dose-dependently mitigated oxidative stress in the R6/2 mouse striatum, as assessed by CellROX signal intensity (Fig. 7A and B) and brain glutathione content (Fig. 7C). CK attenuated phosphorylation of ATM at Ser^{1981} (Fig. 7D) and AMPK-α1 at Thr^{172} (Fig. 7E) in R6/2 mice. Moreover, our data indicated that CK markedly reduced AMPK phosphorylation by the AMPK activator (AICAR, 1 mM) in the mHtt-expressiog cells (Fig. S4). Among the survival-related genes regulated by AMPK, *Bcl2* is involved in the disease progression of HD [29]. Inactivating or preventing nuclear translocation of AMPK-α1 was previously shown to ameliorate mHtt-induced neuronal loss and downregulation of Bcl2 [24]. In the present study, the expression levels of Bcl2 protein were significantly lower in the striatum of R6/2 mice compared to WT mice. Furthermore, chronic treatment with CK significantly upregulated Bcl2 in R6/2 mice (Fig. 7F). Schematic representation of the signaling pathways that mediate the function of CK in rescuing the harmful effect of the ROS/ATM/AMPK-dependent pathway in the presence of mHt (Fig. 7G).

4. Discussion

Age-related neurodegenerative disorders, including AD and HD, consistently show elevated markers of DNA damage [30–34]. Higher phosphorylation of AMPK were also establish in HD and AD. However, the fictional role of the correlation between AMPK-α and ATM in HD pathogenesis has never been reported before. In this

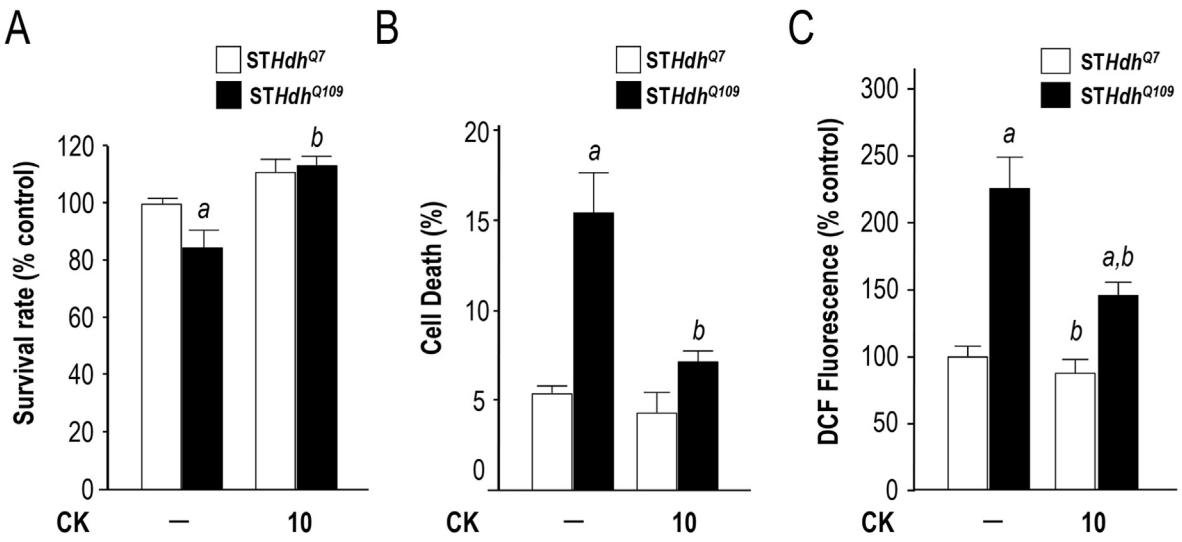

Fig. 4. Compound K (CK) significantly reduces cytotoxicity and oxidative stress in mHtt-expressing cells.

study, we established that mHtt activated ATM in striatal cell lines expressing mHtt and in mice with HD (Figs. 1 and 2). We previously established that the higher ROS and CaMK II level excited by mHTT triggered the over activation of AMPK-α, resulting in HD. Here, we further suggest ATM as an additional harmful factor that upstream of AMPK-α in HD [17,24]. ATM is a key protein involved in the DNA damage response in cells. The role of ATM activation in HD pathogenesis has been demonstrated. Yang and colleagues showed that ATM may be a promising new target in HD, as it can modify the toxicity of the mutant protein that causes HD. They also found that the ATM/γH2AX signaling activity was aberrantly increased in ST*Hdh*^{Q111} cells, BACHD mouse models, and patients with HD. Inhibition of ATM was consistently shown to reduce HD toxicity in cellular and animal models [35]. In this study, we reported that the expression of polyQ-expanded mHtt enhanced the phosphorylation of ATM (Figs. 1 and 2) and AMPK (Fig. 2). The correlation between AMPK and ATM has also been demonstrated. AICAR and IGF-1 phosphorylate the AMPK-α subunit in an ATM-dependent manner [19,36]. Ionizing-radiation-induced DNA damage leads to the activation of ATM, followed by the phosphorylation of AMPK, which mediates cell-cycle arrest via p53 and p21$^{waf/cip}$ expression and the regulation of the G2/M checkpoint in cancer cells [37]. Activation of AMPK by activator (AICAR and metformin) were promoted UVB-induced DNA damage and increased the expression of xeroderma pigmentosum C (XPC) [38]. In this paper, we further propose that ATM is a new upstream of AMPK-α1 in HD. ATM phosphorylated AMPK-α1 via SQ motif in striatal neurons of HD (Fig. 2G). The DNA damage induced by CPT enhanced the activation of AMPK in mHtt-expressing cells (Fig. 3A). ATM regulates DNA repair through the activation of H2AX. Phosphorylation of the Ser^{139} residue of H2AX is coordinated in DNA double-strand breaks [27,28]. We also found that H2AX was activated in mHtt-expressing cells (Fig. 3C and D). In addition, ST*Hdh*^{Q109} cells, which exhibited increased AMPK activity, were more susceptible to CPT-induced DNA damage (Fig. 3). According to our findings we found a novel mechanism by which oxidative-stress-induced DNA damage significantly contributes to the dysfunction of energy sensors in HD.

We previously proposed that the activation of AMPK-α1 potentiates neuronal atrophy and loss induced by mHtt. Our study proved that AMPK was activated in the striatum of R6/2 mice at a late stage, 12 wks and could worsen neuropathological and behavioral phenotypes [24]. A previous study reported that AMPK activators (metformin) may protect mHTT-induced cytotoxicity in the early to intermediate stage of HD [39]. Sanchis et al. showed that metformin in the early stage of HD (3 mo old) may decrease cytotoxicity triggered by mHtt in the cortex and striatum in zQ175 mice [40]. The functional role of AMPK activation in regulation of HD pathogenesis appears to be highly complex and diametrically opposed. We hypothesized that AMPK activation may be mainly protective during the earliest stages (before neuronal degeneration) of HD. However, in the late stages of the disease, activation of AMPK may worsen disease progression in HD.

More than 30 ginsenoside compounds have been identified. Ginsenosides have been previously used to protect against AD and HD symptoms [21]. The molecular mechanisms and medical applications of ginsenosides have attracted much attention in the last few years. The therapeutic potential of ginsenoside has been demonstrated in HD. Rb1, Rc, and Rg5 primary cultures of medium spiny neurons in YAC128 HD mice protecting them from glutamate-induced apoptosis [41]. Rg3 and Rf increased PGC-1α and phosphorylated CREB, reduced p53, Bax, and cleaved caspase-3 in R6/2-derived neural stem cell [42]. Rb1, Rb3, Rg1, Rg3, Rd, and *Panax ginseng* saponin (GTS) reportedly protect against glutamate and 3-nitropropionic acid (3-NP)-induced cell death [43–47]. Ppt reportedly acts to against 3-NP-induced oxidative stress via induced heat shock proteins 70, nuclear factor erythroid 2-related factor 2 (Nrf2), heme oxygenase-1 (HO-1), and NAD(P)H quinone oxidase 1 (NQO1) expression in a rat model of HD [48]. Jang et al. suggested that pre-administration of Korean Red *Panax ginseng* extract (KRGE) inhibited microglial activation, iNOS expression, and proinflammatory cytokine production (interleukin 1β, IL-1β; and interleukin-6, IL-6 and tumor necrosis factor-α, TNF-α) [49]. Jane et al. also reported that gintonin contributes to cell protection from 3-NP-induced striatal toxicity through activating the lysophosphatidic acid receptors and Nrf2 signaling pathway. Gintonin also inhibited the mitogen-activated protein kinase (MAPK) and nuclear factor-κB (NF-κB) signaling pathways [50]. Rg3-enriched KRGE inhibits blood-brain barrier disruption via inhibiting the expression of MitoSOX and 4-hydroxynonenal, and increasing nicotinamide adenine dinucleotide phosphate, oxidase 2 and 4, and NADPH activity in EAE mice (animal model of multiple sclerosis) [51].

The correlation of AMPK and *Panax ginseng* have been demonstrated. *Panax ginseng* C.A. Meyer has been found to protect against AA + iron-induced toxicity by activated LKB1-AMPK signaling

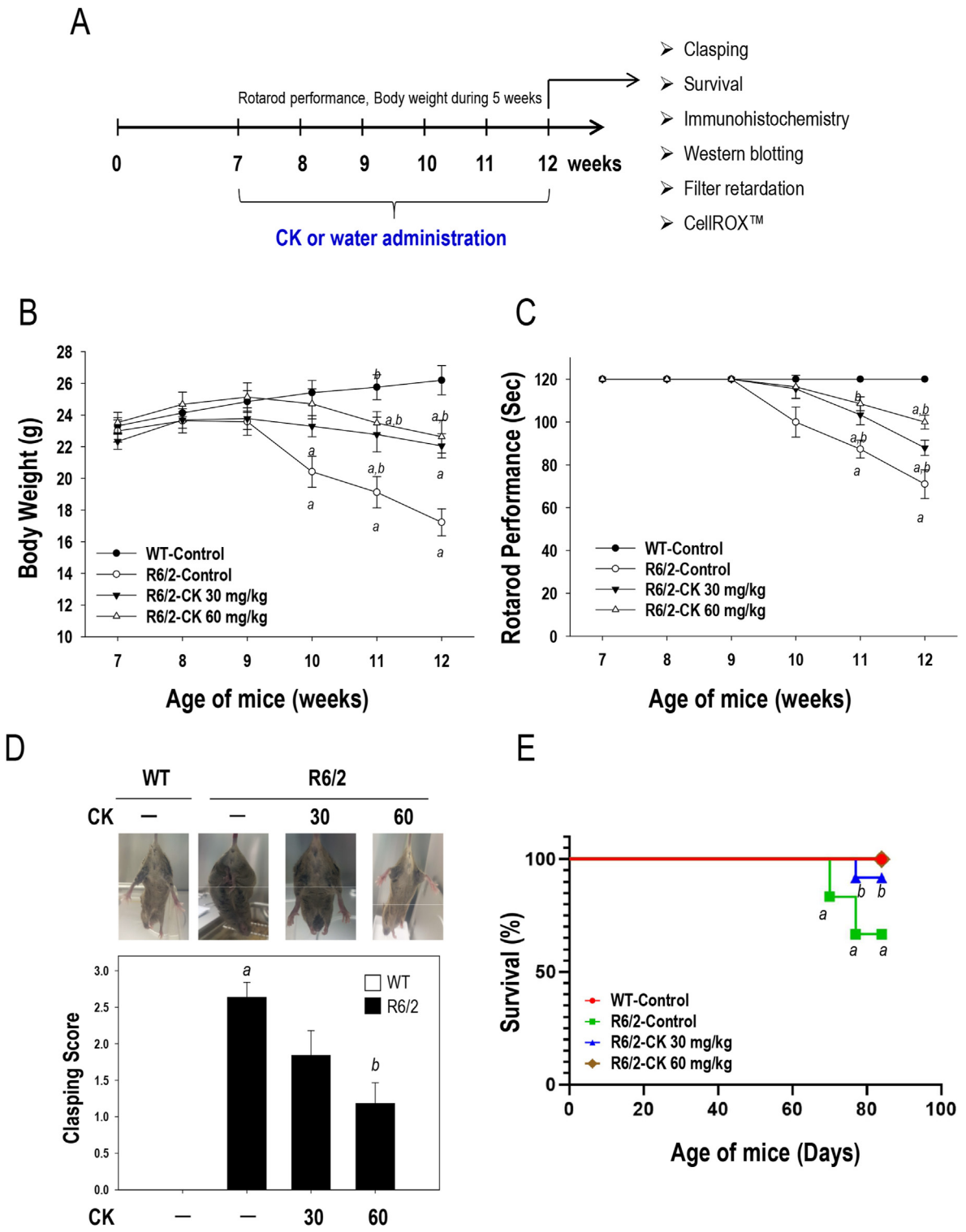

Fig. 5. Compound K (CK) markedly reduces disease progression in the R6/2 mice of HD.

pathway in HepG2 cells [52]. *Panax ginseng* increases insulin secretion and tolerance, glucose uptake and oxidation, and glycogen deposition through the activation of the AMPK pathwas in diabetic rats [53]. 20(S)-ginsenoside Rg3 (S-Rg3) has been found to prevent DEX-induced muscle atrophy through the modulation of the AMPK-FOXO3 signaling pathway [54]. Ginsenoside Rg1 activated the AMPK pathway to increased plasma membrane translocation of glucose transporter type 4 to inhibit dietary-induced obesity and improved obesity-related insulin resistance [55]. However, the correlation between *Panax ginseng* and AMPK in the control nerve system remains unclear.

Higher oxidative stress has been detected in HD and important in HD pathogenesis [56–58]. CK reduces ROS production in neurodegenerative diseases [59] and inflammation via NLRP3

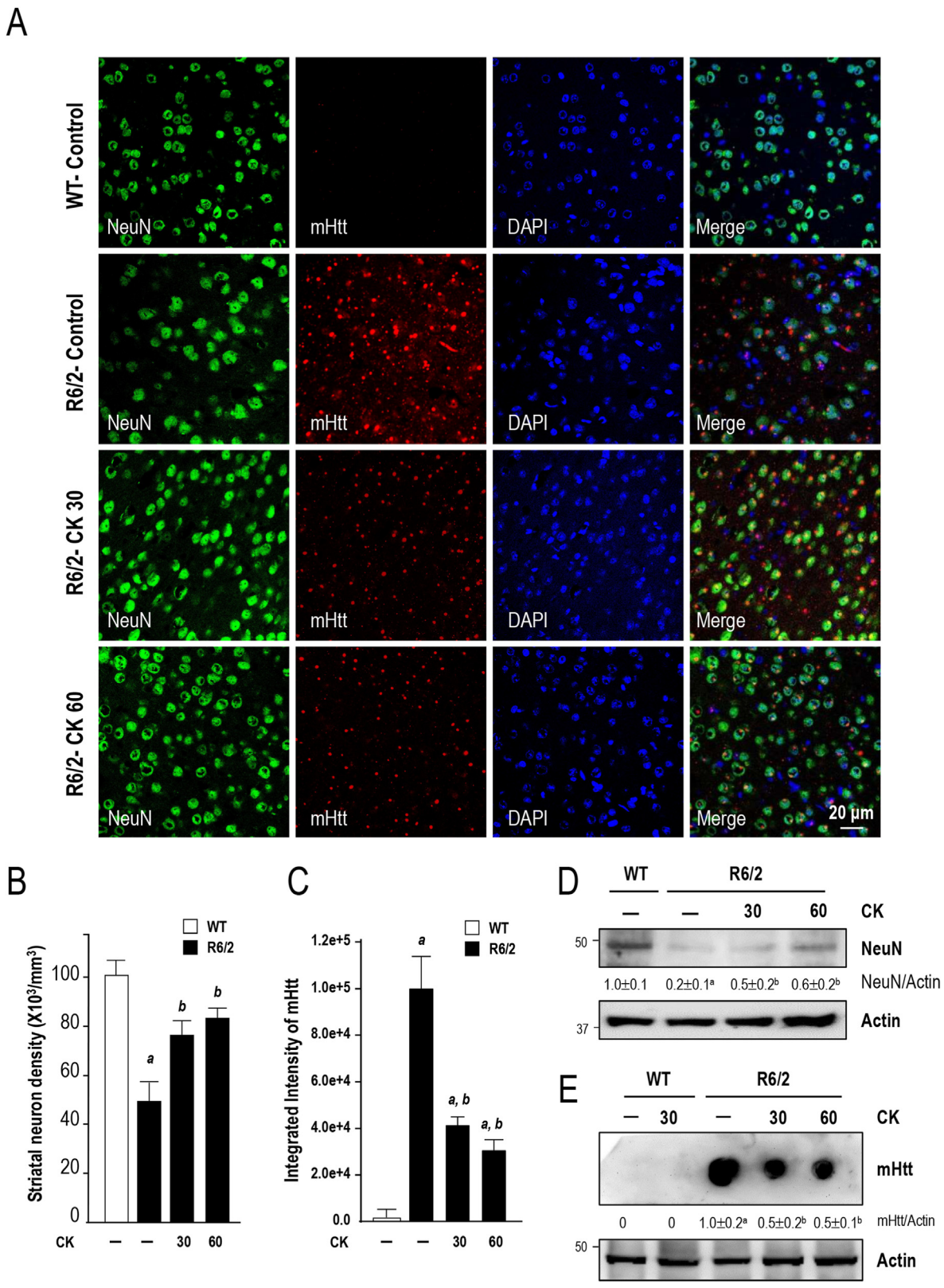

Fig. 6. Compound K (CK) significantly reduces neuronal loss and mHtt aggregation in the R6/2 mice of HD.

pathway in cerebral ischemic injury and high-fat diet-induced diabetic mice [60,61]. CK reduced excitotoxicity and increased spontaneous gamma aminobutyric acid (GABA) release induced by Ca^{2+} [62]. CK also inhibits the release of proinflammatory cytokines such as IL-1β, IL-6, TNF-α, and interleukin-10 (IL-10) in LPS-activated macrophages through the reduction of the NF-κB

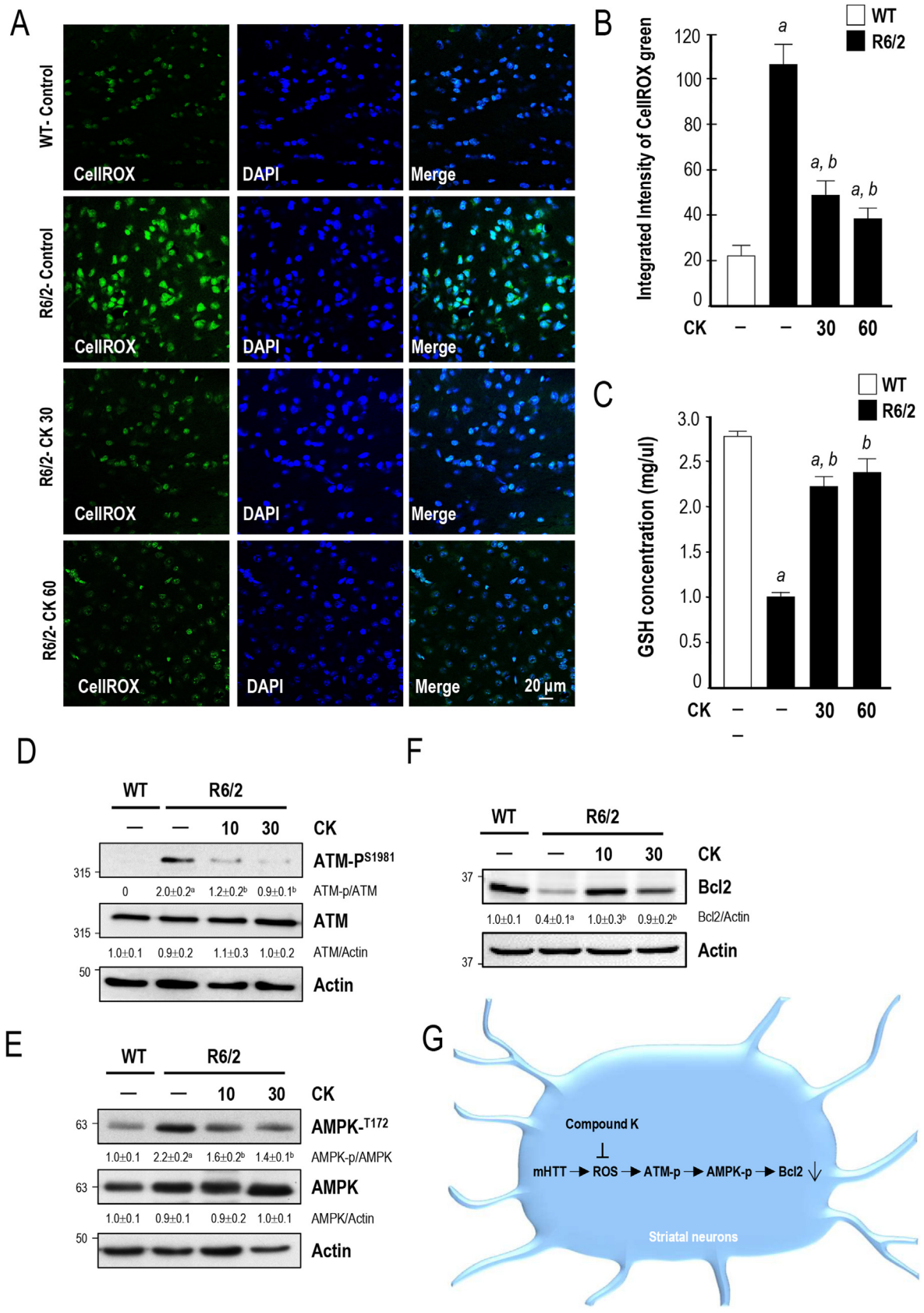

Fig. 7. Compound K (CK) reduces ATM and AMPK overactivation and enhances Bcl2 expression in mHtt-expressing cells and in the R6/2 mice of HD.

signaling pathway [59]. Park et al. suggested that CK suppresses inflammatory molecules by modulating the production of ROS, MAPK, NF-κB, and HO-1 signaling pathways in LPS-stimulated microglia and BV2 cells [63]. Despite these beneficial effects, the detailed protective mechanisms of CK in HD remains unclear that warrant further investigation. As shown in Fig. 4C, CK markedly enhanced cell survival and suppressed ROS production in mHtt-expressing cells. Consistently, the oral administration of CK to R6/2 mice for 5 wks improved neuronal survival, motor function, body weight, and survival rate (Fig. 5). In this study, we further demonstrated that CK suppressed ATM/AMPK activation in HD. The major pathogenic pathways underlying most age-related neurodegenerative disorders (including HD) are the impairment of cellular energy homeostasis and DNA damage in the brain. The molecular determinants and the pathological consequences of the DNA damage repair and energy deficiency observed in HD are currently unknown. Over the past several years, the correlation between oxidative stress and DNA damage has been demonstrated. ATM is induced by oxidative stress via the oxidation of cysteine residues [64]. It is important to point out that we previously reported a positive feedback loops between AMPK and ROS in HD, suggesting that AMPK also positively regulates DNA damage via the enhancement of ROS production. Thus, our results suggest that the accumulation of ROS evoked by a polyQ-expanded mHtt activates ATM, which in turn triggers AMPK, thus further contributing to ROS production in HD. Our findings propose that polyQ expansion induces DNA damage in HD via an ATM−AMPK-dependent pathway. Moreover, activation of ATM improved the phosphorylation level of AMPK in HD. Finally, the oral administration of CK suppressed ATM/AMPK activation and protected striatal neurons in HD. These results propose that CK is useful for the treatment of neurodegenerative disorders.

5. Conclusion

In this study, we demonstrated that the expression of polyQ-expanded mHtt enhanced the phosphorylation of ATM. In addition, ATM phosphorylated AMPK-α in the striatal neurons of mice with HD. Moreover, we demonstrated that oral administration of CK reduced disease progression and markedly enhanced lifespan in a transgenic mouse model (R6/2) of HD through the inhibition of the overactivation of the ATM/AMPK pathway (Fig. 7G). Our study characterized the functional relevance of ATM/AMPK signaling and its role in HD. We believe that the understanding of the functional role of CK in DNA damage and AMPK activation will bring important knowledge for the development of neuroprotective strategies targeting the bioenergetic defects in HD and other age-related diseases.

(A) Immunofluorescence staining of ATM-p (green) and mHtt (EM48, red) in the striatum of the indicated animals (age, 4–12 wks; $n = 6$ for each condition). Nuclei were stained with DAPI (blue). Scale bars, 20 μm. The histograms present the integrated intensity of ATM-p (B) and mHtt (C) in striatal neurons. About 300 cells from each mouse were quantified. Data are expressed as mean ± SEM. [a] $P < 0.05$, WT vs. R6/2 mice. [b] $P < 0.05$ vs. vehicle-treated R6/2 mice. (D) Intrastriatal injection of an ATM inhibitor (ku55933) markedly reduced the phosphorylation of ATM in the striatum of R6/2 mice; 12-wk-old mice were intrastriatally injected with ku55933 (5 mg/kg) or saline. One day post-injection, brain sections were harvested to analyze the expression of ATM-p (green) and mHtt (EM48, red) in the indicated animals ($n = 6$ for each condition). Nuclei were stained with DAPI (blue). The histograms present the integrated intensity of ATM-p (E) and mHtt (F) in striatal neurons. About 300 cells from each mouse were quantified. Data are expressed as mean ± SEM. [b] $P < 0.05$ vs. vehicle-treated R6/2 mice. Scale bars, 20 μm.

(A, C) Cells were incubated with or without an ATM inhibitor (ku55933, 10 μM; mirin, 20 μM) for 24 h (B, D, F) Cells were transfected with a siRNA for ATM for 48 h. Total lysates were assessed by Western blot analyses. (E) Total lysate of ST*Hdh*^{Q7}and ST*Hdh*^{Q109} cells was immunoprecipitated using the indicated antibody and subjected to Western blot analyses. (G) Cells were incubated with or without ATM inhibitor (ku55933, 10 μM) for 24 h or transfected with the indicated construct [AMPK-α1-WT-V5 (WT), AMPK-α1-S413D-V5 (S413D) for 48 h. Total lysate were assessed by Western blot analyses. Molecular mass is indicated in kilodaltons. Results were normalized to those of actin. Data are expressed as the mean ± SEM of three independent experiments. [a] $P < 0.05$, between ST*Hdh*^{Q7} and ST*Hdh*^{Q109}. [b] $P < 0.05$ vs. untreated ST*Hdh*^{Q109} cells.

(A, C) Cells were treated with or without an ATM activator (CPT, 10 μM) at the indicated time points. Total protein lysates were prepared from the striatal cell lines and used in Western blot analyses to determine the levels of the AMPK-p, AMPK-α1, ATM-p, ATM, γH2AX, and actin proteins. The molecular mass is indicated in kilodaltons. Data are expressed as the mean ± SEM of three independent experiments. [a] $P < 0.05$, between ST*Hdh*^{Q7} and ST*Hdh*^{Q109}. [b] $P < 0.05$ vs. untreated ST*Hdh*^{Q109} cells. (B, D) Cells were treated with or without an ATM activator (CPT, 10 μM) for 1 h. Immunofluorescence staining of ATM-p (green), AMPK-p (red), and γH2AX (green) in ST*Hdh*^{Q7} and ST*Hdh*^{Q109} cells was conducted as indicated. Nuclei were stained with DAPI (blue). Scale bars, 20 μm.

(A and B) ST*Hdh*^{Q7} and ST*Hdh*^{Q109} cell death was quantified by the MTT reduction assay and Alamar Blue assay. Cells were incubated for 24 h with CK (10 μM). For both assays, the values were normalized to those of the untreated STHdhQ7 cells. Data are expressed as the mean ± SEM of three independent experiments. a $P < 0.05$, STHdhQ7 vs. STHdhQ1^{09} cells. [b] $P < 0.05$ CK-treated vs. untreated ST*Hdh*^{Q109} cells. (C) To measure cellular ROS levels, cells were incubated with H_2DCFDA (50 μM) for 30 min followed by treatment with CK (10 μM) for 24 h. Data are expressed as the mean ± SEM of three independent experiments. [a] $P < 0.05$, specific comparison between ST*Hdh*^{Q7} and ST*Hdh*^{Q109} cells. [b] $P < 0.05$ vs. untreated ST*Hdh*^{Q109} cells.

Mice were treated daily with CK or vehicle for 5 wks from the age of 7 wks. (A) Schematic representation of the experimental procedure and behavioral test (B) Rotarod performance, (C) body weight, and (D) clasping ($n = 12$ for each condition) were assessed. Data are expressed as the mean ± SEM. [a] $P < 0.05$, WT vs. R6/2 mice. [b] $P < 0.05$, CK- vs. vehicle-treated R6/2 mice. (E) Survival assessment ($P < 0.05$, Kaplan–Meier survival analysis).

Mice were treated daily with CK or vehicle for 5 wks from the age of 7 wks. (A) Brain sections of 12-wk-old mice were stained with NeuN and EM48. The number of neurons (NeuN; green) and the level of mHtt aggregation (EM48; red) in the striatum of the indicated mice ($n = 6$ for each condition) were quantified. Nuclei were stained with DAPI (blue). The histograms show the number of striatal neurons (B) and the integrated intensity of mHtt (C). About 500 cells from each mouse were quantified. Data are expressed as the mean ± SEM. Scale bars, 20 μm [a] $P < 0.05$, WT vs. R6/2 mice. [b] $P < 0.05$ vs. vehicle-treated R6/2 mice. (D) Striatal lysates were analyzed by Western blot analysis. The molecular mass is indicated in kilodaltons. (E) The amount of mHtt aggregation in striatal lysates was analyzed by a filter retardation assay. The insoluble aggregates retained on the filters were detected using an anti-mHtt antibody. The molecular mass is indicated in kilodaltons. Data are expressed as the mean ± SEM of three independent experiments. [a] $P < 0.05$, WT vs. R6/2 mice. [b] $P < 0.05$, CK- vs. vehicle-treated R6/2 mice.

Mice were treated daily with CK or vehicle for 5 wks, starting from 7 wks of age. (A) Brain sections from 12-wk-old mice were stained with CellROX™ Green Reagent (green) to identify ROS; nuclei were stained with DAPI (blue). Scale bar, 20 μm. (B) Quantification of CellROX™ Green fluorescence intensity in the striatum of the indicated mice ($n = 3$ for each condition; at least 100 cells from each animal were quantified). Data are expressed as the mean ± SEM. [a] $P < 0.05$ WT vs. R6/2 mice. [b] $P < 0.05$ CK- vs. vehicle-treated R6/2 mice. (D-F) Striatal lysates were analyzed by Western blot analysis to determine the levels of the ATM-p, AMPK-p, Bcl2, and actin proteins. The molecular mass is indicated in kilodaltons. Data are expressed as the mean ± SEM of three independent experiments. [a] $P < 0.05$, WT vs. R6/2 mice. [b] $P < 0.05$, CK- vs. vehicle-treated R6/2 mice. (G) Schematic representation of the signaling pathways that mediate the function of compound K (CK) in rescuing the harmful effect of the ROS/ATM/AMPK-dependent pathway in the presence of mHtt.

Funding

This work was supported by grants from the Ministry of Science and Technology of Taiwan [grant numbers MOST 106-2311-B-029-005, MOST 107-2311-B-029-002, MOST 109-2622-B-029-001, MOST 108-2314-B-037-038-MY3] and Kaohsiung Medical University Hospital [grant numbers KMUH 108-8R61, KMUH 109-9R72] in Taiwan.

Declaration of competing interest

All the authors declare that they have no conflicts of interest.

Acknowledgments

We are very grateful to Drs. Elena Cattaneo and Yijuang Chern for providing the striatal cell lines (STHdh Q7and STHdhQ109). We would like to thank National Laboratory Animal Center for providing the B6CBAFI/J mice.

Appendix A. Supplementary data

Supplementary data to this article can be found online at https://doi.org/10.1016/j.jgr.2021.11.003.

References

[1] Martin JB, Gusella JF. Huntington's disease. Pathogenesis and management. N Engl J Med 1986;315:1267–76.
[2] Group., s D C R TH. A novel gene containing a trinucleotide repeat that is expanded and unstable on Huntington's disease chromosomes. The Huntington's Disease Collaborative Research Group. Cell 1993;72:971–83.
[3] Landles C, Bates GP. Huntingtin and the molecular pathogenesis of Huntington's disease. Fourth in molecular medicine review series. EMBO Rep 2004;5:958–63.
[4] Buckley NJ, Johnson R, Zuccato C, Bithell A, Cattaneo E. The role of REST in transcriptional and epigenetic dysregulation in Huntington's disease. Neurobiol Dis 2010.
[5] Li H, Li SH, Yu ZX, Shelbourne P, Li XJ. Huntingtin aggregate-associated axonal degeneration is an early pathological event in Huntington's disease mice. J Neurosci 2001;21:8473–81.
[6] Lin YS, Chen CM, Soong BW, Wu YR, Chen HM, Yeh WY, Wu DR, Lin YJ, Poon PW, Cheng ML, Wang CH, Chern Y. Dysregulated brain creatine kinase is associated with hearing impairment in mouse models of Huntington disease. J Clin Invest 2011;121:1519–23.
[7] Chiang MC, Chen HM, Lee YH, Chang HH, Wu YC, Soong BW, Chen CM, Wu YR, Liu CS, Niu DM, Wu JY, Chen YT, Chern Y. Dysregulation of C/EBPalpha by mutant Huntingtin causes the urea cycle deficiency in Huntington's disease. Hum Mol Genet 2007;16:483–98.
[8] Klapstein GJ, Fisher RS, Zanjani H, Cepeda C, Jokel ES, Chesselet MF, Levine MS. Electrophysiological and morphological changes in striatal spiny neurons in R6/2 Huntington's disease transgenic mice. J Neurophysiol 2001;86:2667–77.
[9] Martindale D, Hackam A, Wieczorek A, Ellerby L, Wellington C, McCutcheon K, Singaraja R, Kazemi-Esfarjani P, Devon R, Kim SU, Bredesen DE, Tufaro F, Hayden MR. Length of huntingtin and its polyglutamine tract influences localization and frequency of intracellular aggregates. Nat Genet 1998;18:150–4.
[10] Vonsattel JP, Myers RH, Stevens TJ, Ferrante RJ, Bird ED, Richardson Jr EP. Neuropathological classification of Huntington's disease. J Neuropathol Exp Neurol 1985;44:559–77.
[11] Long YC, Zierath JR. AMP-activated protein kinase signaling in metabolic regulation. J Clin Invest 2006;116:1776–83.
[12] Stein SC, Woods A, Jones NA, Davison MD, Carling D. The regulation of AMP-activated protein kinase by phosphorylation. Biochem J 2000;345 Pt 3:437–43.
[13] Hurley RL, Barre LK, Wood SD, Anderson KA, Kemp BE, Means AR, Witters LA. Regulation of AMP-activated protein kinase by multisite phosphorylation in response to agents that elevate cellular cAMP. J Biol Chem 2006;281:36662–72.
[14] Raney MA, Turcotte LP. Evidence for the involvement of CaMKII and AMPK in Ca2+-dependent signaling pathways regulating FA uptake and oxidation in contracting rodent muscle. J Appl Physiol 2008;104:1366–73.
[15] Tsuboi T, da Silva Xavier G, Leclerc I, Rutter GA. 5'-AMP-activated protein kinase controls insulin-containing secretory vesicle dynamics. J Biol Chem 2003;278:52042–51.
[16] Cai Y, Martens GA, Hinke SA, Heimberg H, Pipeleers D, Van de Casteele M. Increased oxygen radical formation and mitochondrial dysfunction mediate beta cell apoptosis under conditions of AMP-activated protein kinase stimulation. Free Radic Biol Med 2007;42:64–78.
[17] Ju TC, Chen HM, Chen YC, Chang CP, Chang C, Chern Y. AMPK-alpha1 functions downstream of oxidative stress to mediate neuronal atrophy in Huntington's disease. Biochim Biophys Acta 2014;1842:1668–80.
[18] Giuliano P, De Cristofaro T, Affaitati A, Pizzulo GM, Feliciello A, Criscuolo C, De Michele G, Filla A, Avvedimento EV, Varrone S. DNA damage induced by polyglutamine-expanded proteins. Hum Mol Genet 2003;12:2301–9.
[19] Suzuki A, Kusakai G, Kishimoto A, Shimojo Y, Ogura T, Lavin MF, Esumi H. IGF-1 phosphorylates AMPK-alpha subunit in ATM-dependent and LKB1-independent manner. Biochem Biophys Res Commun 2004;324:986–92.
[20] Fu X, Wan S, Lyu YL, Liu LF, Qi H. Etoposide induces ATM-dependent mitochondrial biogenesis through AMPK activation. PLoS One 2008;3:e2009.
[21] Cho IH. Effects of Panax ginseng in neurodegenerative diseases. J Ginseng Res 2012;36:342–53.
[22] Cattaneo E, Conti L. Generation and characterization of embryonic striatal conditionally immortalized ST14A cells. J Neurosci Res 1998;53:223–34.
[23] Ho CL, Li LH, Weng YC, Hua KF, Ju TC. Eucalyptus essential oils inhibit the lipopolysaccharide-induced inflammatory response in RAW264.7 macrophages through reducing MAPK and NF-kappaB pathways. BMC Complement Med Ther 2020;20:200.
[24] Ju TC, Chen HM, Lin JT, Chang CP, Chang WC, Kang JJ, Sun CP, Tao MH, Tu PH, Chang C, Dickson DW, Chern Y. Nuclear translocation of AMPK-alpha1 potentiates striatal neurodegeneration in Huntington's disease. J Cell Biol 2011;194:209–27.
[25] Liu FC, Wu GC, Hsieh ST, Lai HL, Wang HF, Wang TW, Chern Y. Expression of type VI adenylyl cyclase in the central nervous system: implication for a potential regulator of multiple signals in different neurotransmitter systems. FEBS Lett 1998;436:92–8.
[26] Traven A, Heierhorst J. SQ/TQ cluster domains: concentrated ATM/ATR kinase phosphorylation site regions in DNA-damage-response proteins. Bioessays 2005;27:397–407.
[27] Burma S, Chen BP, Murphy M, Kurimasa A, Chen DJ. ATM phosphorylates histone H2AX in response to DNA double-strand breaks. J Biol Chem 2001;276:42462–7.
[28] Sharma A, Singh K, Almasan A. Histone H2AX phosphorylation: a marker for DNA damage. Methods in molecular biology, vol. 920. NJ: Clifton; 2012. p. 613–26.
[29] Zhang Y, Ona VO, Li M, Drozda M, Dubois-Dauphin M, Przedborski S, Ferrante RJ, Friedlander RM. Sequential activation of individual caspases, and of alterations in Bcl-2 proapoptotic signals in a mouse model of Huntington's disease. J Neurochem 2003;87:1184–92.
[30] Lu XH, Mattis VB, Wang N, Al-Ramahi I, van den Berg N, Fratantoni SA, Waldvogel H, Greiner E, Osmand A, Elzein K, Xiao J, Dijkstra S, de Pril R, Vinters HV, Faull R, Signer E, Kwak S, Marugan JJ, Botas J, Fischer DF, Svendsen CN, Munoz-Sanjuan I, Yang XW. Targeting ATM ameliorates mutant Huntingtin toxicity in cell and animal models of Huntington's disease. Sci Transl Med 2015;6. 268ra178.
[31] Bogdanov MB, Andreassen OA, Dedeoglu A, Ferrante RJ, Beal MF. Increased oxidative damage to DNA in a transgenic mouse model of Huntington's disease. J Neurochem 2001;79:1246–9.
[32] Mao P, Reddy PH. Aging and amyloid beta-induced oxidative DNA damage and mitochondrial dysfunction in Alzheimer's disease: implications for early intervention and therapeutics. Biochim Biophys Acta 2011;1812:1359–70.
[33] Coppede F, Migliore L. DNA damage and repair in Alzheimer's disease. Curr Alzheimer Res 2009;6:36–47.
[34] Anderson AJ, Su JH, Cotman CW. DNA damage and apoptosis in Alzheimer's disease: colocalization with c-Jun immunoreactivity, relationship to brain area, and effect of postmortem delay. J Neurosci 1996;16:1710–9.

[35] Markus, A. A., Parsons, J. R., Roex, E. W., de Voogt, P. & Laane, R. W. Modeling aggregation and sedimentation of nanoparticles in the aquatic environment, Sci Total Environ. 506–507, 323-329.
[36] Sun Y, Connors KE, Yang DQ. AICAR induces phosphorylation of AMPK in an ATM-dependent, LKB1-independent manner. Mol Cell Biochem 2007;306:239–45.
[37] Sanli T, Steinberg GR, Singh G, Tsakiridis T. AMP-activated protein kinase (AMPK) beyond metabolism: a novel genomic stress sensor participating in the DNA damage response pathway. Cancer Biol Ther 2010;15:156–69.
[38] Wu CL, Qiang L, Han W, Ming M, Viollet B, He YY. Role of AMPK in UVB-induced DNA damage repair and growth control. Oncogene 2013;32:2682–9.
[39] Vazquez-Manrique RP, Farina F, Cambon K, Dolores Sequedo M, Parker AJ, Millan JM, Weiss A, Deglon N, Neri C. AMPK activation protects from neuronal dysfunction and vulnerability across nematode, cellular and mouse models of Huntington's disease. Hum Mol Genet 2016;25:1043–58.
[40] Sanchis A, Garcia-Gimeno MA, Canada-Martinez AJ, Sequedo MD, Millan JM, Sanz P, Vazquez-Manrique RP. Metformin treatment reduces motor and neuropsychiatric phenotypes in the zQ175 mouse model of Huntington disease. Exp Mol Med 2019;51:1–16.
[41] Wu J, Jeong HK, Bulin SE, Kwon SW, Park JH, Bezprozvanny I. Ginsenosides protect striatal neurons in a cellular model of Huntington's disease. J Neurosci Res 2009;87:1904–12.
[42] Lee M, Ban JJ, Won BH, Im W, Kim M. Therapeutic potential of ginsenoside Rg3 and Rf for Huntington's disease. In Vitro Cell Dev Biol Anim 2021;57:641–8.
[43] Kim YC, Kim SR, Markelonis GJ, Oh TH. Ginsenosides Rb1 and Rg3 protect cultured rat cortical cells from glutamate-induced neurodegeneration. J Neurosci Res 1998;53:426–32.
[44] Lian XY, Zhang Z, Stringer JL. Protective effects of ginseng components in a rodent model of neurodegeneration. Ann Neurol 2005;57:642–8.
[45] Kim JH, Kim S, Yoon IS, Lee JH, Jang BJ, Jeong SM, Lee JH, Lee BH, Han JS, Oh S, Kim HC, Park TK, Rhim H, Nah SY. Protective effects of ginseng saponins on 3-nitropropionic acid-induced striatal degeneration in rats. Neuropharmacology 2005;48:743–56.
[46] Kim SE, Shim I, Chung JK, Lee MC. Effect of ginseng saponins on enhanced dopaminergic transmission and locomotor hyperactivity induced by nicotine. Neuropsychopharmacology 2006;31:1714–21.
[47] Yang X, Chu SF, Wang ZZ, Li FF, Yuan YH, Chen NH. Ginsenoside Rg1 exerts neuroprotective effects in 3-nitropronpionic acid-induced mouse model of Huntington's disease via suppressing MAPKs and NF-kappaB pathways in the striatum. Acta Pharmacol Sin 2021;42:1409–21.
[48] Gao Y, Chu SF, Li JP, Zhang Z, Yan JQ, Wen ZL, Xia CY, Mou Z, Wang ZZ, He WB, Guo XF, Wei GN, Chen NH. Protopanaxtriol protects against 3-nitropropionic acid-induced oxidative stress in a rat model of Huntington's disease. Acta Pharmacol Sin 2015;36:311–22.
[49] Jang M, Lee MJ, Kim CS, Cho IH. Korean red ginseng extract attenuates 3-nitropropionic acid-induced Huntington's-like symptoms. Evid Based Complement Alternat Med; 2013. p. 237207. 2013.
[50] Jang M, Choi JH, Chang Y, Lee SJ, Nah SY, Cho IH. Gintonin, a ginseng-derived ingredient, as a novel therapeutic strategy for Huntington's disease: activation of the Nrf2 pathway through lysophosphatidic acid receptors. Brain Behav Immun 2019;80:146–62.
[51] Lee MJ, Choi JH, Oh J, Lee YH, J G, Chang BJ, Nah SY, Cho IH. Rg3-enriched Korean Red Ginseng extract inhibits blood-brain barrier disruption in an animal model of multiple sclerosis by modulating expression of NADPH oxidase 2 and 4. J Ginseng Res 2021;45:433–41.
[52] Dong GZ, Jang EJ, Kang SH, Cho IJ, Park SD, Kim SC, Kim YW. Red ginseng abrogates oxidative stress via mitochondria protection mediated by LKB1-AMPK pathway. BMC Compl Alternative Med 2013;13:64.
[53] Abdelazim A, Khater S, Ali H, Shalaby S, Afifi M, Saddick S, Alkaladi A, Almaghrabi OA. Panax ginseng improves glucose metabolism in streptozotocin-induced diabetic rats through 5' adenosine monophosphate kinase up-regulation. Saudi J Biol Sci 2019;26:1436–41.
[54] Wang M, Jiang R, Liu J, Xu X, Sun G, Zhao D, Sun L. 20(s)ginseonsideRg3 modulation of AMPK/FoxO3 signaling to attenuate mitochondrial dysfunction in a dexamethasoneinjured C2C12 myotubebased model of skeletal atrophy in vitro. Mol Med Rep 2021;23.
[55] Li JB, Zhang R, Han X, Piao CL. Ginsenoside Rg1 inhibits dietary-induced obesity and improves obesity-related glucose metabolic disorders. Braz J Med Biol Res 2018;51:e7139.
[56] Perez-Severiano F, Rios C, Segovia J. Striatal oxidative damage parallels the expression of a neurological phenotype in mice transgenic for the mutation of Huntington's disease. Brain Res 2000;862:234–7.
[57] Tabrizi SJ, Workman J, Hart PE, Mangiarini L, Mahal A, Bates G, Cooper JM, Schapira AH. Mitochondrial dysfunction and free radical damage in the Huntington R6/2 transgenic mouse. Ann Neurol 2000;47:80–6.
[58] Segovia J, Perez-Severiano F. Oxidative damage in Huntington's disease. Methods in molecular biology (Clifton, NJ 2004;277:321–34.
[59] Song W, Guo Y, Jiang S, Wei L, Liu Z, Wang X, Su Y. Antidepressant effects of the ginsenoside metabolite compound K, assessed by behavioral despair test and chronic unpredictable mild stress model. Neurochem Res 2018;43:1371–82.
[60] Oh J, Kim JS. Compound K derived from ginseng: neuroprotection and cognitive improvement. Food Funct 2016;7:4506–15.
[61] Song W, Wei L, Du Y, Wang Y, Jiang S. Protective effect of ginsenoside metabolite compound K against diabetic nephropathy by inhibiting NLRP3 inflammasome activation and NF-kappaB/p38 signaling pathway in high-fat diet/streptozotocin-induced diabetic mice. Int Immunopharm 2018;63:227–38.
[62] Bae MY, Cho JH, Choi IS, Park HM, Lee MG, Kim DH, Jang IS. Compound K, a metabolite of ginsenosides, facilitates spontaneous GABA release onto CA3 pyramidal neurons. J Neurochem 2010;114:1085–96.
[63] Park JS, Shin JA, Jung JS, Hyun JW, Van Le TK, Kim DH, Park EM, Kim HS. Anti-inflammatory mechanism of compound K in activated microglia and its neuroprotective effect on experimental stroke in mice. J Pharmacol Exp Therapeut 2012;341:59–67.
[64] Guo Z, Kozlov S, Lavin MF, Person MD, Paull TT. ATM activation by oxidative stress, vol. 330. New York, NY: Science; 2010. p. 517–21.